MASTER (MA)

Effect of End Group Identity on RAFT Polymers for Lipid Nanodisc Stabilisation

Neville, George

Award date:
2019

Awarding institution:
University of Bath

Electronic Supplementary Information

Effect of End Group Identity on RAFT Polymers for Lipid Nanodisc Stabilisation

George M. Neville, Karen J. Edler, Gareth J. Price

1.0 Experimental

1.1 Polymer Synthesis & Nanodisc Preparation

1.1.1 Materials

Before polymerisation, styrene (*Sigma Aldrich*, purity ≥ 99%), was passed through a disposable, pre-packed column (*Sigma Aldrich)* to remove the inhibitor 4-tert-butylcatechol. The comonomer, maleic anhydride (MAnh) (puriss, purity ≥ 99%), the initiator, 2,2'-Azobis(2-methylpropionitrile) (AIBN), the RAFT agent, 2-(dodecylthiocarbonothioylthio)-2-methylpropionic acid (DDMAT) (purity 98%, HPLC grade), and the solvent, 1,4-dioxane were purchased from *Sigma Aldrich* and not purified further before use. The commercial SMA variant, SMA 2000, was provided by *Cray Valley*. The lipid species, t-2-dimystoyl-*sn*-glycero-3-phosphocholine (DMPC) (purity ≥ 99%) and 1,2-dipalmitoyl-*sn*-glycero-3-phosphocholine (DPPC) (purity ≥ 99%), were purchased from *Sigma Aldrich*, and deuterated 1,2-dimyristoyl-d54-*sn*-glycero-3-phosphocholine (d-DMPC) (purity > 99%) from *Avanti Polar Lipids*. Lauroyl peroxide (LPO) was purchased from *BDH Chemicals LTD.*, and mono and dibasic sodium phosphate (purity ≥ 99%) from *Acros Organics*. All other solvents used were purchased from *Sigma Aldrich* and used as received.

1.1.2 RAFT polymerisation of SMAnh

In accordance with the protocol adapted from Harrison and Wooley,[1] the monomers, styrene and maleic acid, the initiator, AIBN, and the RAFT agent, DDMAT, were dissolved in 1,4-dioxane in the molar ratios found in Table S1. Several polymers with molecular weights ranging between 4.5 – 8.0 kDa were kindly synthesised and supplied by Ella R. Shiliday.

Table S1 Molar ratios used to synthesise the 2:1 styrene-maleic acid copolymer SMAnh R

Reagent	Mr / gmol^{-1}	Mass / g	Mol	Predicted M_n / kDa[a]
Styrene	104.15	7.0021	0.0672	
MAnh	98.06	2.8273	0.0288	
1,4-Dioxane	88.11	21.000	0.2383	6
AIBN	164.21	0.3031	0.0018	
DDMAT	364.63	0.6335	0.0017	

[a] $Mn(pre) = (\frac{mol(styrne)\times Mr(styrne)\times conversion}{mol(DDMAT)}) + (\frac{mol(MAnh)\times Mr(MAnh)\times conversion}{mol(DDMAT)}) + Mr(DDMAT)$, where conversion is assumed to be 100%.

RAFT is a variation on reversible deactivation radical polymerisation techniques typically used in producing polymers of low polydispersity and predictable molecular weights, a generalised reaction mechanism of which is presented in Fig. S1.

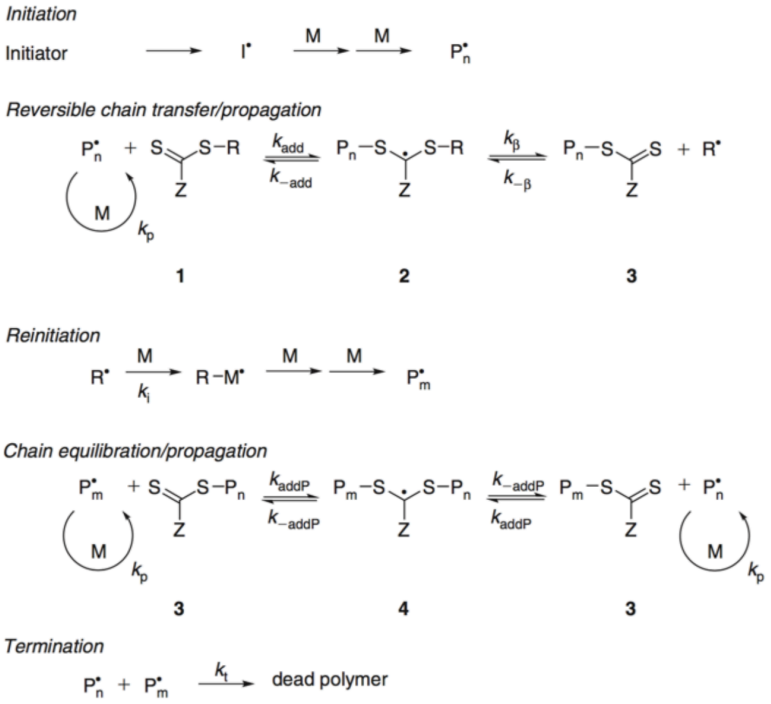

Fig. S1 General reaction scheme for RAFT polymerisation.

Reaction mixtures were sealed in a round bottomed flask before degassing with nitrogen and three subsequent freeze-thaw cycles, under vacuum, to purge oxygen that could potentially poison the initiator species and effect the resultant molecular weight. This was then covered with foil to exclude light, before heating to 60 °C for 24 hours. Polymers were precipitated in 500 ml diethyl ether at 0 °C. For d-SMA, the procedure was identical, except for the substitution of d_6-styrene for styrene.

1.1.3 Hydrolysis of SMAnh to SMA

SMAnh was hydrolysed to SMA in accordance with the procedure outlined by Hall *et al.*,[2] whereby a 10% (wt/v) polymer solution was made with 1M aqueous NaOH and heated to 120 °C for 2 hours, under reflux. Polymers were then precipitated by acidification to pH 3.0 with 4M aqueous HCl, and centrifugation using an *Eppendorf 5804R* centrifuge for 15 minutes at 21°C at 8000 rpm. The supernatant was removed and the pellet washed with water and centrifuged again a further three times. To further purify the polymer, the pellet was then dissolved in 0.6 M NaOH before repeating the precipitation and washing procedure. The precipitate was then dissolved in 0.6 M NaOH and adjusted to pH 8.0, to ensure sufficient deprotonation of MA moieties for nanodisc formation, before freeze drying (*Virtis SP Scientific*), for a minimum of 24 hours.

1.1.4 End Group Modification of SMA (R) to SMA (RR)

RAFT polymerisations incur a resulting polymer end group dependent on the RAFT agent used. Here, this is a thiolcarbonylthio group, specifically dodecylthiocarbonothioylthio, which is hydrophobic. A method for exchanging this end group for a hydrophilic cyanoisoproypyl group was adapted from the work of Chen *et al.*,[3] a reaction scheme for which can be found in Fig. S2. Previous to these developments, only part exchange of the RAFT end group in styrenic polymers was possible as the polymeric radicals were a poorer leaving group than the cyanoisopropyl radicals afforded by AIBN. By introducing LPO, a better leaving group, not only is this problem avoided, but the likelihood of chain combination is reduced due to an increased availability of cyanoisopropyl radicals. As suggested, here, an excess of AIBN (20 molar equivalents) and LPO (2 molar equivalents) were added

to a 3% (wt/v) polymer solution in toluene. This was then degassed with nitrogen following three freeze-thaw cycles to exclude radical-poisoning oxygen, before being heated to 80 °C for 4 hours. The solution was then dried under nitrogen before hydrolysis without the need for further modification.

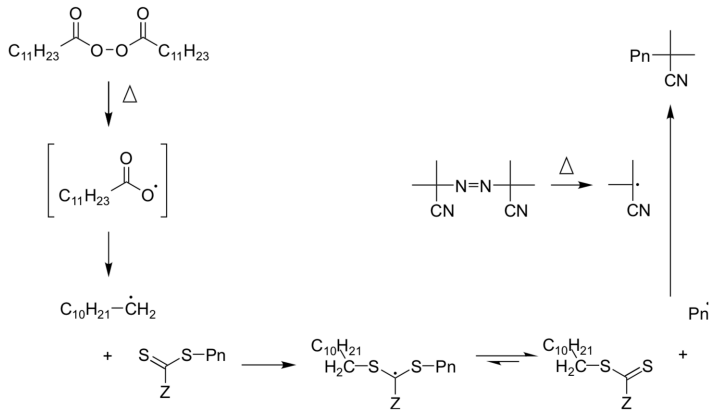

Fig. S2 Reaction scheme for end group exchange from thiocarbonylthio to cyanoisopropyl.

1.1.5 Nanodisc Preparation

Nanodiscs were prepared in a 50 mM (0.2M NaCl) phosphate buffer solutions (PBS) stabilised at pH 8.0, within the range nanodiscs have been previously been reported to be stable. Lipid species (5.0 mg), whether DMPC, d-DMPC, or DPPC, were dissolved in 0.679 ml PBS and sonicated in two 10 second bursts, with a 50% duty cycle, separated by a 15 second rest period to prevent overheating. 15 mg of polymers in 0.231 ml PBS were then added to this solution, resulting in a nanodisc solution consisting of 1.65% (wt/v) polymer and 0.55% (wt/v) lipid. An immediate indication of successful nanodisc formation is garnered from the loss of turbidity upon the addition of polymer solutions.

1.2 Polymer & Nanodisc Characterisation

1.2.1 Fourier Transform Infrared Spectroscopy (FTIR)

All FTIR spectra were recorded using a *Perkin Elmer* desktop spectrometer with polymer samples at room temperature in solid state. Each spectrum was scanned for 14 runs between wavenumbers 500 to 4000 cm-1.

1.2.2 ^{1}H & ^{13}C Nuclear Magnetic Resonance Spectroscopy (NMR)

^{1}H NMR spectra were recorded using an *Agilent* 500 MHZ NMR spectrometer. SMAnh and SMA polymers were dissolved in d_6-acetone and D_2O, respectively, at room temperature, at high concentrations (40 mgml^{-1}). Spectra were processed in *Mestrelab MNova* 11.0 software, where spectra were baseline corrected to allow integration of peak area, and line broadening was systematically employed to ease analysis given multiple monomer environments. ^{13}C spectra were conducted with the same method but lengthened acquisition times to improve signal-to-noise ratios.

1.2.3 ^{1}H-^{15}N Heteronuclear Multiple Bond Correlation (HMBC) NMR

Experiments were conducted on a 500MHz *Bruker AV III HD* spectrometer, equipped with a liquid nitrogen cooled *Prodigy BBO* cryoprobe, operating at 500.2 MHz for ^{1}H spectra, and 50.7 MHz for ^{15}N spectra. Spectra were recorded at room temperature using 192 gradient increments, each containing 192 scans, taking 20.5

hours. Experiments were optimised for a ^{1}H-^{15}N coupling of 3 Hz.

1.2.4 Diffusion Ordered Spectroscopy (DOSY) ^{1}H NMR

All spectroscopy was conducted on a *Bruker AV* 500 MHz spectrometer at room temperature with anhydride polymer samples dissolved in d_6-acetone (20 $mgml^{-1}$). DOSY operates by the acquisition of a series of spin-echoes, each with a different gradient of magnetic field strength between the top and bottom of the sample. This causes different speeds of nuclear procession, dependent on the location of molecules within the sample. When a 180 ° pulse is applied, if molecules have not moved during this time, the magnetic field experienced will not have changed and procession would be at the same rate as the rotating frame, returning signal (Fig S3a). Hence, those that diffuse, lose signal, and as the field strength gradient is steepened across the series, faster diffusing nuclei will loose signal to a greater degree (Fig S3b). This effect is described by Equation 1:

$$I = I_0 e^{-D\gamma^2 g^2 \delta^2 (\Delta - \frac{\delta}{3})} \quad (\mathbf{1})$$

Where I is the signal intensity, I_0 the signal intensity before gradient application, D the diffusion coefficient, γ the gyromagnetic ratio, g the gradient strength, δ the time the gradient is applied for and Δ the time allowed for diffusion. Therefore, a plot of $\ln(I)$ vs. g^2 gives the diffusion coefficient. Here, 8 gradient steps were used to ensure reliable measurement of *D*.

a

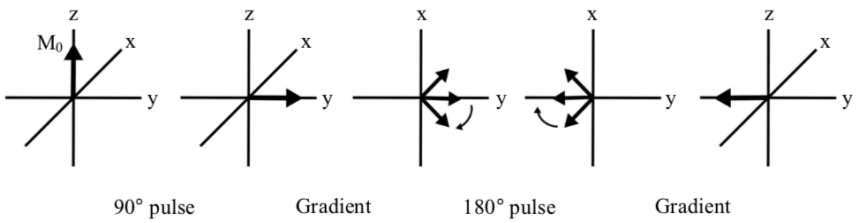

b

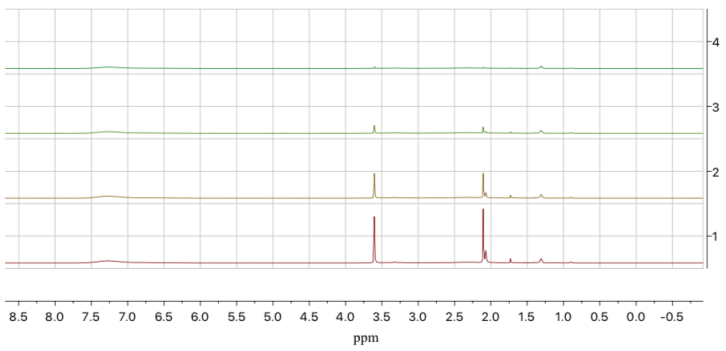

Fig. S3 (a) Spin-echo series applied in DOSY and (b) resultant loss of signal as gradient steepened.

1.2.5 UV-vis Spectroscopy

Spectra were recorded using an *Agilent Cary 60* UV-vis spectrometer and a quartz cuvette to mitigate absorbance in the styrene range.

1.2.6 Gel Permeation Chromatography

2 mgml^{-1} SMAnh polymer solutions in THF were submitted to an *Agilent GPC 1260 Infinity* for run times of 40 minutes per sample. Unfortunately, aqueous GPC was not available at the time of experiment, however, it can be presumed molecular weights are maintained post hydrolysis to SMA. Elution times of solutes were inversely proportional to molecular weight, and detected using variation in refractive index from blank THF. Chromatograms were calibrated against a polystyrene standard: Whilst a reportedly acceptable standard for SMAnh,[4] it is possible that interactions between MAnh and the stationary phase may have caused deviations from absolute molecular weights. *Agilent GPC/SEC* software was used to extract M_n and PDI values from chromatograms.

1.2.7 Dynamic Light Scattering

DLS was conducted using a *Malvern Zetasizer Nano Series*, using either disposable plastic cuvettes for size, or folded capillary zeta cells for zeta potential. Where particles are adequately dilute, and therefore can not interact, particles size can be ascertained from fluctuations in scattering intensity at a fixed angle. Here, fluctuation is caused by interference from changing distances between scatterers and the detector, hence allowing characterisation of diffusion coefficients, directly relating to the hydrodynamic radius (Fig. S4).

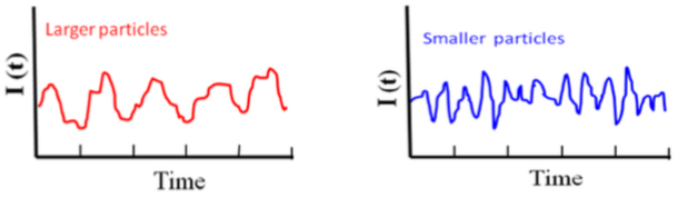

Fig. S4 Variation to scatting intensity over time for (left) large and (right) small particles in solution.

Zetasizer software was calibrated with constants from *p*(styrene-*alt*-maleic acid) in PBS (50 mM, 0.2 M NaCl). Samples were diluted to a concentration of 0.1%, sufficient to assume an infinite dilution regime. Prior to all measurements, solutions were passed through a 0.45 μm *Millex Millipore* membrane filter to remove contaminant scatters such as dust. Measurements were taking using backscattering (θ = 173 °) and λ = 633 nm. To allow valid comparison, all values reported were a volume particle size distribution – opposed to intensity based, which emphasises larger particles, or number based, which emphasises smaller particles. In all cases, five sets of measurements were taken, each with at least 12 runs, to ensure satisfactory cumulate fits.

1.2.8 Pendant Drop Tensiometry

Tensiometry was conducted and processed using *FTA 32* surface tension image analysis software. Syringes needles were prepared by extensive washing with water, ethanol and acetone to remove contaminants. Aggregate samples at relevant concentrations were then passed through these needles to produce a small hanging droplet which is then imaged at a typical rate of 10 images per second to ensure a good average measurement (Fig. S5a). An iterative convergence calculation is then used to fit the shape of the drop to Equation 2, where γ is surface tension, $\Delta\rho$ is the difference in density of the light and heavy phase, g is gravitational acceleration, D_e is the maximum diameter (Fig. S5b), and H is a correction coefficient between the horizontal and vertical D_e values:

$$\gamma = \frac{\Delta\rho g D_e^2}{H} \qquad (2)$$

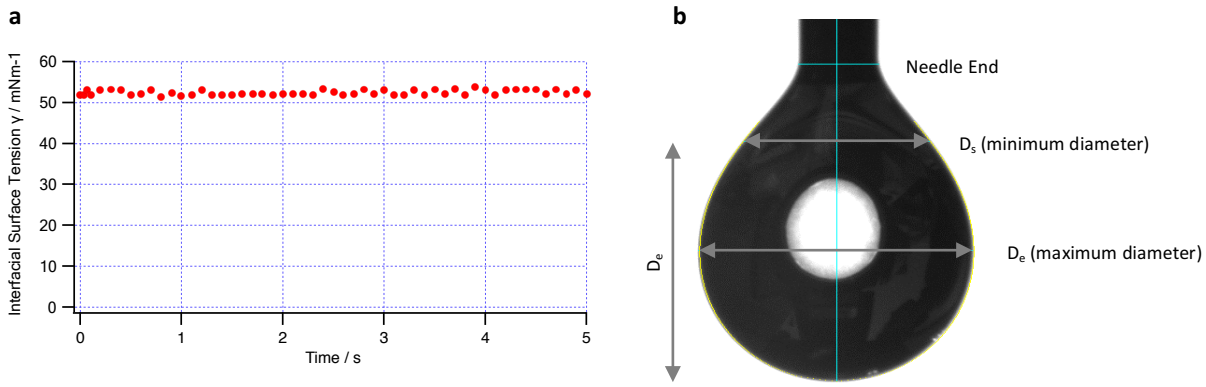

Fig S5 (a) Resultant plot of interfacial surface tension against time from *FTA 32* software. (b) Single image from *FTA 32* software where droplet shape has been outlined and divided into sections including needle end, D_s, and D_e.

The software was calibrated against 18.2 ΩM ultra-filtered water with a surface tension of 72.15 mNm^{-1} with air. The magnification and distance between the camera and the drop was calibrated against the diameter of the needle, known to be 0.6419 mm from manufacturing specifications. In the case of dodecane to PBS measurements, the sample drop was suspended in a cuvette of dodecane, utilising a straight, opposed to curved, needle given the lesser density of dodecane compared to water (Table 2).

Table S2 Densities of light and heavy phase used in calculation for respective interfacial surface tension measurements

Experiment	Phase	Density ρ / gcc^{-1}
Air-PBS	Air (Light)	0.0011
	PBS (Heavy)	1.0000
Dodecane-PBS	Dodecane (Light)	0.7500
	PBS (Heavy)	1.0000

1.2.9 Transmission Electron Microscopy (TEM)

SMALP and aggregate samples were prepared in PBS at 1.65% (wt/v) polymer concentrations, before being float cast onto a glow discharged (*Edwards S150B* sputter coater) carbon film electron microscopy grid. Due to high concentration samples, casting times were accordingly restricted to approximately 15 seconds. Samples were then negatively stained using uranyl acetate filtered through a 0.22 μm *Millex Millipore* membrane driven filter. Imaging was performed using *JEM-2100* transmission electron microscope at an operating voltage of 200 kV. Subsequent image processing, such as particle sizing, was carried out in *Fiji Image-J* software.

1.2.9 Small Angle X-ray Scattering (SAXS) and Neutron Scattering (SANS)

SAXS and SANS can be used to interrogate the structure, size and composition of particles in solution. X-rays interact with electron density, whereas neutrons with the strong force of nuclei, where incident radiation can be scattered in an elastic or inelastic manor. Inelastic scattering occurs when incident energy is lost, and hence scattered radiation is incoherent, and does not provide structural information. Elastic scattering, however, is coherent, and interferes to give a scattering pattern which may be analysed. A general schematic of a scattering experiment is provided in Fig. S6.

As distance within a scattering pattern is relative to the wavelength of radiation used, rather than using angle (2θ), the vector q is adopted to render patterns wavelength independent (Equation 3). Overall scattering intensity, $I(q)$, at any given q is described by Equation 4, where ρ is the scattering length density (SLD), V, is particle volume, B_{inc} is incoherent scattering intensity, and $F(q)$ and $S(q)$ are the form factor and structure factor,

respectively. *F(q)* described the shape of the particle, at low-*q*, gradient is predominantly related to size, at mid-*q*, the cross-sectional structure (*i.e.* sphere, cylinder, *etc.*) and at high-*q*, surface structure. *S(q)* arises from particle interactions and is superimposed over *F(q)*. At low-*q*, a steep gradient is indicative of aggregation whereas a decreasing gradient would indicate repulsive interactions. Therefore, for systems sufficiently dilute, it is assumed that *S(q)* = 1. Furthermore, polydispersity is apparent from scattering patterns as the overall pattern is the sum average of the properties of each particle.

$$q = \frac{4\pi}{\lambda} \times \sin(\theta) \tag{3}$$

$$I(q) = N_p V_p^2 (\rho_p - \rho_s)^2 F(q) S(q) + B_{inc} \tag{4}$$

Here, SANS was performed at the *ISIS Neutron and Muon Source* (Didcot, UK), on the *Larmor* and *Zoom* instruments. SAXS was collected at the *Diamond Light Source* (Didcot, UK). All data was fit using a combination of the open-source software *SASview* using the Levenberg-Marquardt method and the *NIST* SANS analysis package[ref] within *Igor Pro 6* from *Wavemetrics*.

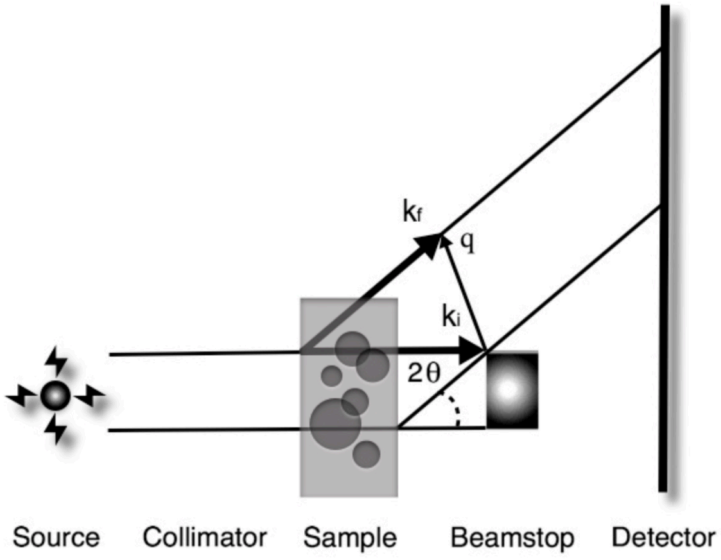

Fig. S6 General schematic for the SANS or SAXS instrumental set-up.

2.0 Supplementary Data

2.1 NMR Spectra

2.1.1 ^{1}H NMR

Typically, polymers express broad NMR signals due to the increased number of environments for any given molecular unit. Integration to identify the ratio of styrene to maleic acid in SMA polymers, has however, been widely adopted.[2] Here, for example, the integral of the styrenic peak, *a*, between δ = 7.60-6.05, 1.00, was divided by the five hydrogens the peak is associated with (Fig. S7). Similarly, the peak associated with maleic anhydride, *b*, 0.20, was divided by 2 to give 0.1. Overall, this gives a styrene to maleic acid ratio of 0.2:0.1, therefore 2:1. Also identifiable is the thiocarbonylthio group afford by RAFT synthesis at δ = 0.8,[5] used during eventual ^{1}H DOSY NMR experiments to trace the cleaving of the end group into solution.

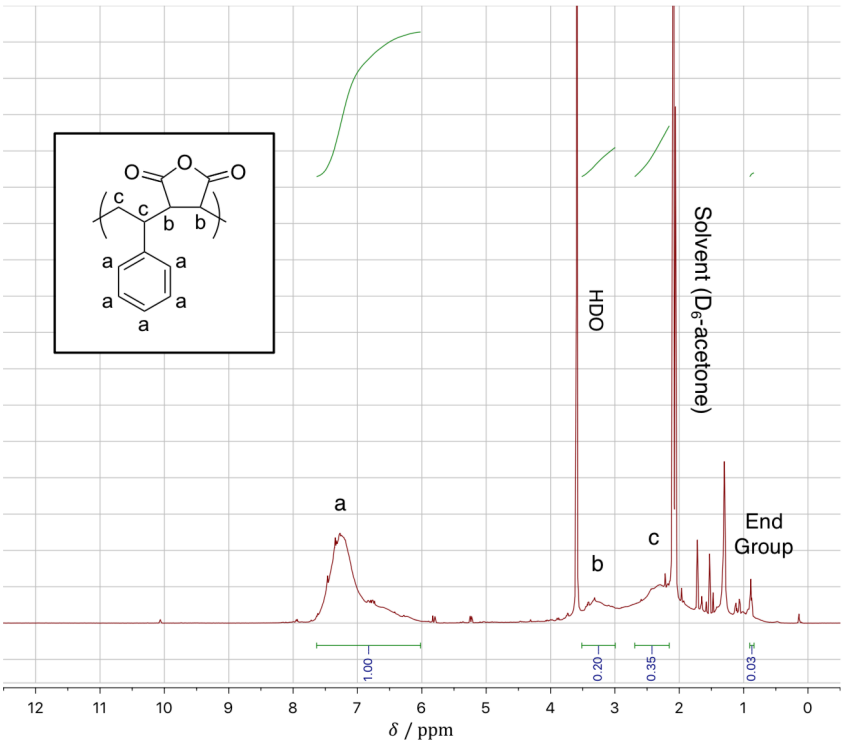

Fig. S7 ^{1}H NMR spectrum of SMAnh R. (d_6-acetone): δ 7.60-6.05 (5H, borad, H_a), 3.05-3.50 (2H, broad, H_b), 2.15-2.70 (2H, broad H_c), 0.87-0.90 (3H, t, DDMAT end group).

2.1.2 ^{13}C NMR

^{13}C NMR was used to observe the introduction of a Sty-*alt*-MA-*homo*-Sty architecture, introduced by RAFT synthesis. It has been previously identified that peaks at 36.3 and 40.5 ppm refer to the alternating block, and those at 42.0 and 51.8 ppm, the styrene homoblock.[6] As seen in Fig. S8, SMAnh R contains this structure. Whilst SMAnh 2000 contains similar peaks, these are comparatively broadened, and the spectrum completely lacks the alternating peak at 36.3 ppm. Moreover, SMAnh R lacks the peak at 38.1 ppm, found in SMAnh 2000, representing semi-alternating, randomised structure.

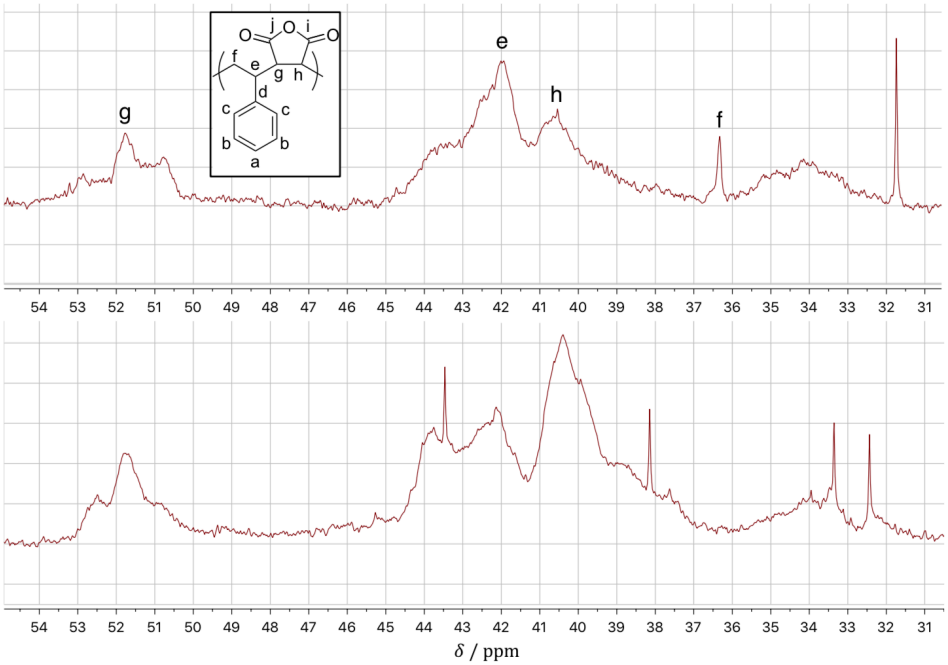

Fig. S8 ^{13}C NMR spectra of (top) SMAnh R and (bottom) SMA 2000 highlight polymer topology.

2.1.3 ^{1}H-^{15}N HMBC NMR

HMBC NMR was used in an attempt to confirm the presence of non-hydrolysed nitrile groups in SMA RR, as it is known that nitriles would normally undergo basic hydrolysis in the conditions used here to hydrolyse SMAnh. From the spectra (Fig. S9) it can be seen that both anhydride polymers contain two nitrogen peaks at approximately ^{1}H 1.0 - 1.5 ppm (^{15}N 100 – 150 ppm).

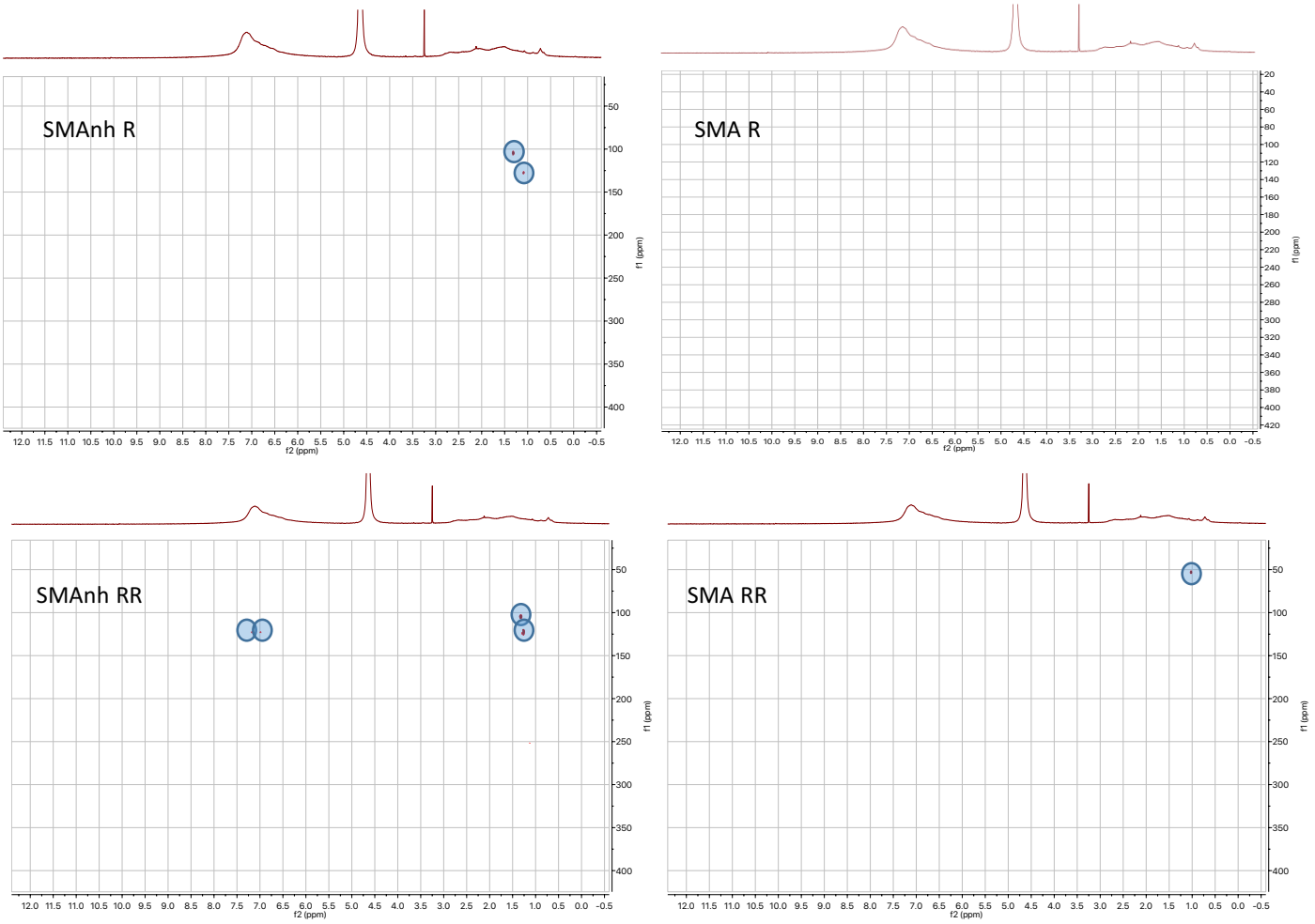

Fig. S9 ^{1}H-^{15}N HMBC spectra for anhydride polymers (left) and acid polymers (rights) for (top) SMA/nh R and (bottom) SMA/nh RR.

These likely relate to small molecules free in solution, such as unreacted AIBN radicals, as they do not correspond to polymeric peaks and had singlet structure. SMAnh RR has two additional peaks at approximately ^{15}N 125 ppm, plausibly representing a nitrile, attached to styrene polymer units (^{1}H 7.5 – 6.0 ppm). Post hydrolysis, however, it can be seen that these peaks are no longer present. SMA RR, does however, contain an additional peak (^{15}N 50 ppm) in comparison to SMA R, which has none. This peak is most likely an amine, although could feasibly represent a nitrile. Therefore, the results of these experiments are inconclusive as to whether the proposed cyanoisopropyl group survives hydrolysis, but does point to the preservation of some form of nitrogen environment. Caution must be taken when interpreting these results, as the sensitivities used were uncommonly high in order to detect nitrogen atoms that are expected to be at least 4 bonds away from the nearest hydrogen nucleus. Future research may benefit from employing mass spectrometry as an alternative analysis technique.

2.2 FTIR

FTIR spectra were primarily used to confirm the successful hydrolysis of SMAnh species to SMA. As seen in Fig. S10, evidence of the transformation of MAnh to MA is observed from the loss of peaks at 1217 cm^{-1} and 1075 cm^{-1} representing C-O-C ether bonds. Moreover, symmetric and assymetric carbonyl stretching frequencies at 1854 and 1773 cm^{-1} are shifted to a lower wavenumber at 1563 cm-1. Alternately, aromatic C-H stretching frequencies at approximately 3000, 1493 and 1453 cm^{-1}, representing styrene, are unchanged post reaction, corroborating that hydrolysis affects MAnh units only. Similar spectra were obtained for all copolymers.

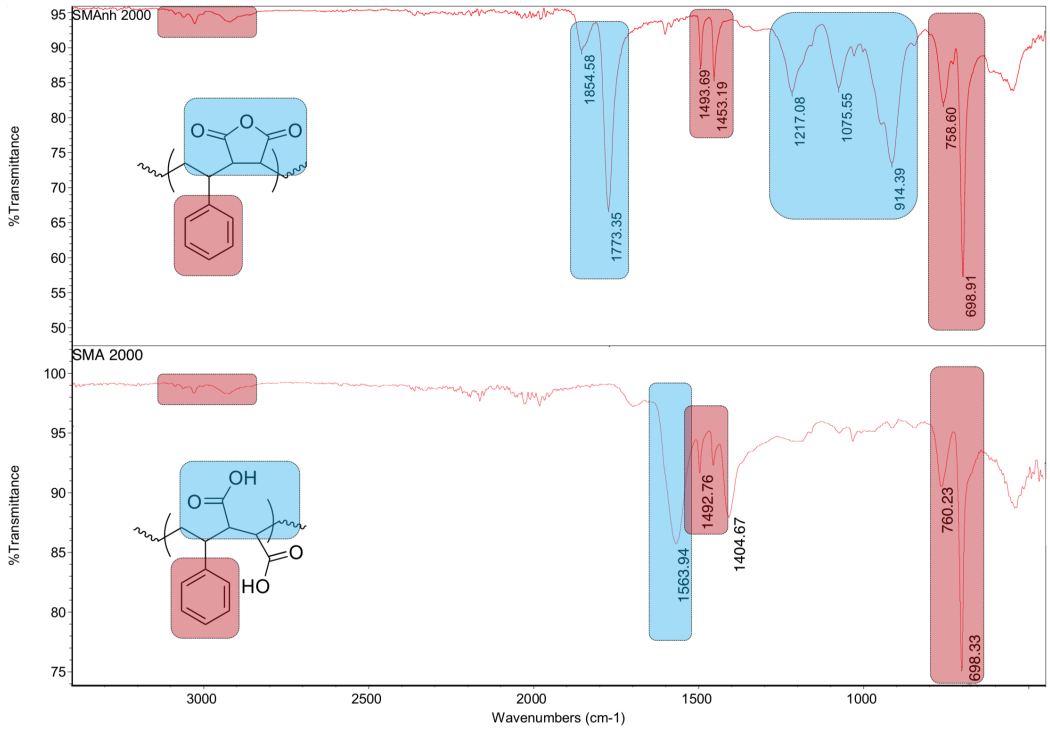

Fig. S10 FTIR spectra for (top) SMAnh 2000, before hydrolysis to (bottom) SMA 2000, with stretching frequencies highlighted that are associated with (red) styrene units and (blue) maleic anhydride/acid units.

2.3 DLS

Here, DLS data that was excluded from the main report for clarity, has been tabulated.

2.3.1 Zeta Potential

High zeta potential – either positive or negative – is indicative of greater colloidal stability. Measurements here were taken to model subsequent *S(q)* in SANS data, where charge parameters were set to 20 mV.

Table S3 Polymer aggregate and SMALP nanodisc zeta potentials.

Sample	Zeta Potential mV
SMA R Aggregate (1.2% wt/v)	-24.7 ± 1.9
SMA RR Aggregate (1.2% wt/v)	-24.8 ± 1.3
SMA 2000 Aggregate (1.2% wt/v)	-24.9 ± 1.9
SMA R Nanodisc	-17.98 ± 0.32
SMA RR Nanodisc	-20.18 ± 0.54
SMA 2000 Nanodisc	-12.9 ± 1.2

2.3.2 Copolymer Aggregate Size

Table S4 Aggregate diameter and PDI.

Aggregate Sample	Concentration / %(wt/v)	Temperature / °C	Diameter / nm[a]	PDI[a]
SMA R	0.02	25	10.24 ± 3.89	0.52 ± 0.18
SMA R	0.02	45	9.81 ± 0.92	0.28 ± 0.15
SMA R	0.02	65	10.78 ± 1.53	0.25 ± 0.05
SMA RR	0.02	25	0.71 ± 0.04	0.66 ± 0.12
SMA RR	0.02	45	2.14 ± 1.90	0.67 ± 0.17
SMA RR	0.02	65	0.77 ± 0.03	0.93 ± 0.07
SMA 2000	0.02	25	2.01 ± 0.82	0.43 ± 0.04
SMA 2000	0.02	45	2.69 ± 0.94	0.28 ± 0.12
SMA 2000	0.02	65	1.45 ± 0.68	0.59 ± 0.23
SMA R	0.10	25	13.14 ± 0.20	0.14 ± 0.01
SMA R	0.10	45	12.07 ± 0.38	0.13 ± 0.02
SMA R	0.10	65	12.23 ± 0.20	0.14 ± 0.01
SMA RR	0.10	25	13.16 ± 0.54	0.54 ± 0.01
SMA RR	0.10	45	13.04 ± 0.75	0.56 ± 0.01
SMA RR	0.10	65	12.85 ± 0.69	0.52 ± 0.01
SMA 2000	0.10	25	2.56 ± 0.02	0.18 ± 0.02
SMA 2000	0.10	45	3.31 ± 0.23	0.30 ± 0.01
SMA 2000	0.10	65	2.06 ± 0.02	0.39 ± 0.09
SMA R (A)	1.65	25	10.95 ± 0.55	0.22 ± 0.02
SMA R (B)	1.65	25	9.6 ± 1.2	0.29 ± 0.01
SMA R (C)	1.65	25	15.65 ± 0.35	0.16 ± 0.01
SMA RR (A)	1.65	25	120.8 ± 4.96	0.21 ± 0.01
SMA RR (B)	1.65	25	133.25 ± 0.76	0.24 ± 0.01
SMA RR (C)	1.65	25	14.4 ± 1.0	0.58 ± 0.01

[a] Error reported at 95% C.I. from average of 5 sets of at least 12 scans.

2.3.3 SMALP Nanodiscs Size

Table S5 SMALP nanodisc diameters and PDI.

Nanodisc Sample	Lipid Species	Temperature / °C	Diameter / nm[a]	PDI[a]
SMA R	DMPC	25	18.9 ± 1.0	0.48 ± 0.01
SMA R	DMPC	45	12.8 ± 1.0	0.26 ± 0.01
SMA R	DMPC	65	11.2 ± 1.6	0.25 ± 0.01
SMA RR	DMPC	25	14.86 ± 0.24	0.45 ± 0.01
SMA RR	DMPC	45	14.14 ± 0.15	0.45 ± 0.01
SMA RR	DMPC	65	12.74 ± 0.44	0.44 ± 0.01
SMA 2000	DMPC	25	5.92 ± 0.11	0.27 ± 0.02
SMA 2000	DMPC	45	5.37 ± 0.14	0.23 ± 0.06
SMA 2000	DMPC	65	4.91 ± 0.19	0.19 ± 0.05
SMA R	DPPC	25	88 ± 38	0.24 ± 0.01
SMA RR	DPPC	25	16.99 ± 0.27	0.23 ± 0.01
SMA 2000	DPPC	25	9.78 ± 0.30	0.14 ± 0.01
SMA R (A)	DMPC	25	19.78 ± 0.05	0.21 ± 0.01
SMA R (B)	DMPC	25	18.69 ± 0.13	0.17 ± 0.01
SMA R (C)	DMPC	25	20.71 ± 0.82	0.18 ± 0.01
SMA RR (A)	DMPC	25	16.20 ± 0.20	0.58 ± 0.01
SMA RR (B)	DMPC	25	16.34 ± 0.72	0.61 ± 0.02
SMA RR (C)	DMPC	25	15.75 ± 0.61	0.58 ± 0.01

[a] Error reported at 95% C.I. from average of 5 sets of at least 12 scans.

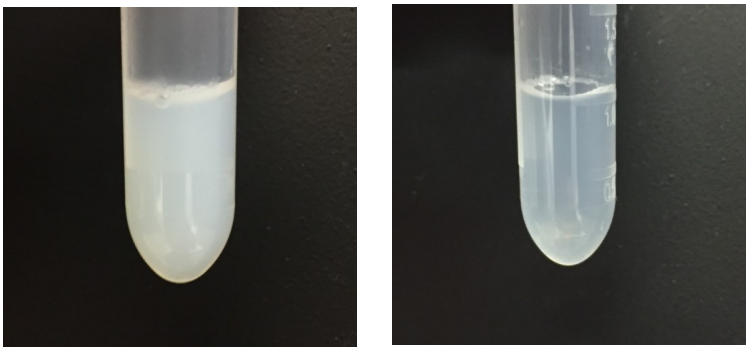

Fig. S11 Images of DPPC solutions at least 24 hours after addition of (left) SMA R and (right) SMA RR, highlighting apparent inability of SMA R to solubilise DPPC.

2.4 SANS

Parameters held during fitting are listed in Table S6. All polydispersity values were taken from DLS measurements and held. SLD of aggregate shell based on incorporating all polymeric MA units – although future research may wish to attempt to fit data to 50:50 MA-Sty shell. SLDs of other components were calculated by Equation 5:

$$Nb = \frac{N_A \times \rho}{MW} \times \sum_i b_i \quad (5)$$

Where N_A *is* Avogadro's number, ρ, is density, *MW*, is molecular weight, and b_i is the coherent scattering length of each atom in the compound.

Table S6 Model parameters held during fitting.

Parameter	Held Value
SLD Nanodisc Face	1.84×10^{-6} Å^{-2}
Hydration Nanodisc Face[a]	0.57 %
Nanodisc Face Thickness[a]	0.8 nm
SLD h-SMA R[b]	1.99×10^{-6} Å^{-2}
SLD h-SMA RR[b]	2.02×10^{-6} Å^{-2}
SLD d-SMA R[b]	4.91×10^{-6} Å^{-2}
SLD d-SMA RR[b]	4.93×10^{-6} Å^{-2}
SLD h-Polymer Sty Core[b]	1.68×10^{-6} Å^{-2}
SLD h-Polymer MA Shell[b]	2.96×10^{-6} Å^{-2}
SLD d-polymer Sty core[b]	6.21×10^{-6} Å^{-2}
SLD d-polymer MA shell[b]	2.96×10^{-6} Å^{-2}
SLD 100% D_2O Solvent	6.29×10^{-6} Å^{-2}
SLD 70% D_2O Solvent	4.23×10^{-6} Å^{-2}
SLD 50% D_2O Solvent	2.86×10^{-6} Å^{-2}
Charge[c]	20 mV
Monovalent Salt Concentration[c]	0.25 M
Temperature[c]	298 K
Dielectric Constant[c]	78

[a] From literature.[7] [b] As calculated from Equation 5. [c]Used to fit structure factor of spherical aggregates and nanodiscs only.

2.9.1 Copolymer Aggregates

SMA R aggregates were fit to a core shell sphere model with a polydisperse radius, whereas SMA RR aggregates were fit using a core shell cylinder model with polydisperse radius and length. Values held during fitting are listed in Table S7. Fit parameters for SMA R and SMA RR aggregates are found in Table S8 and Table S9 respectively, with fit graphs in Fig. 12 and 13, respectively.

Table S7 SMA R and SMA RR aggregate held parameters.

Parameter	Held Value
PDI SMA R Radius	0.23
PDI SMA RR Radius	0.56
PDI SMA RR Length	0.56

Table S8 Fit parameters for SMA R spherical aggregates

Parameter	Fit Value
Scale	0.004 ± 0.002
Radius	3 ± 2 nm
Shell Thickness	0.5 ± 0.2 nm
SLD Shell[a]	$4.9 \pm 0.9\times10^{-6}$ Å^{-2}; $3.0 \pm 0.9\times10^{-6}$ Å^{-2}
Mol. Frac. Solvent in Rim	0.60 ± 0.25

[a] (left) value for 100% D_2O contrast and (right) for 50% D_2O contrast.

Table S9 Fit parameters for SMA RR cylindrical aggregates

Parameter	Fit Value
Volume Fraction	0.005 ± 0.002
Core Radius	3.6 ± 0.2
Length	1.5 ± 0.4 nm
Shell Thickness	0.9 ± 0.2 nm
SLD Shell[a]	$3.5 \pm 0.5\times10^{-6}$ Å^{-2}; $2.9 \pm 0.5\times10^{-6}$ Å^{-2}
Mol. Frac. Solvent in Shell	0.2 ± 0.1

[a] (left) value for 100% D_2O contrast and (right) for 50% D_2O contrast.

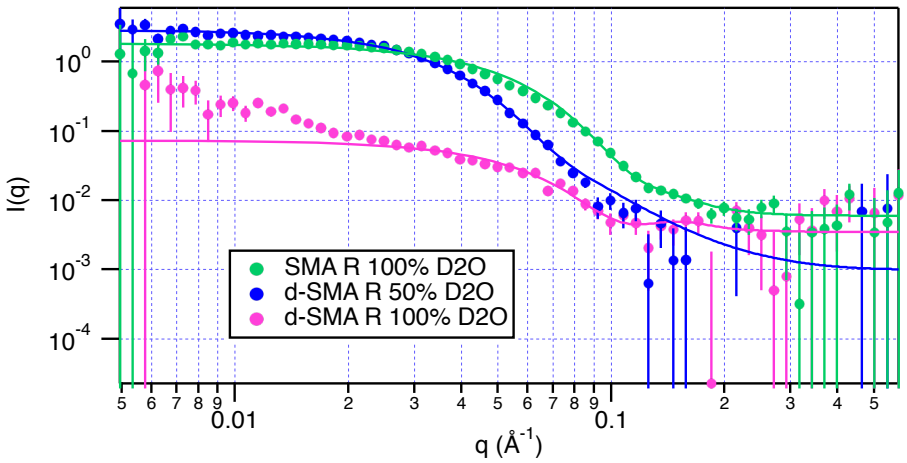

Fig. S12 Fit SANS data for spherical SMA R aggregates. (green) SMA R 100% D_2O (blue) d-SMA R 50% D_2O (pink) d-SMA R 100% D_2O.

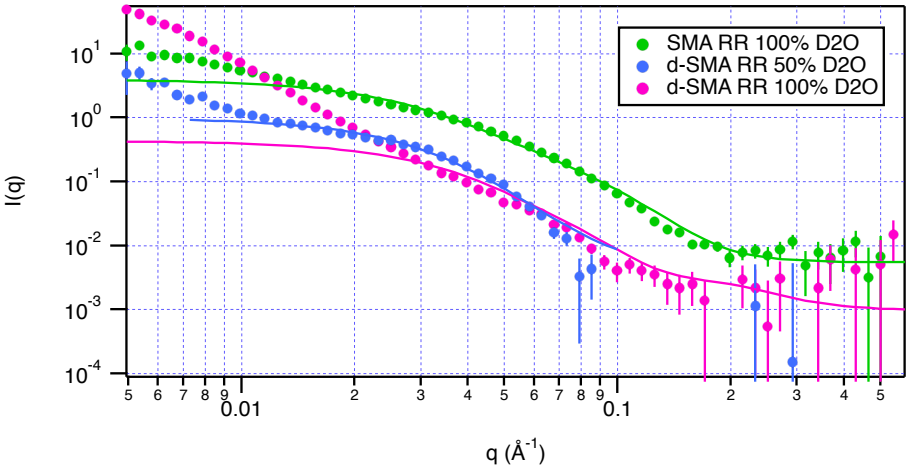

Fig. S13 Fit SANS data for cylindrical SMA RR aggregates. (green) SMA RR 100% D_2O (blue) d-SMA RR 50% D_2O (pink) d-SMA RR 100% D_2O.

2.9.2 SMALP Nanodiscs

2.9.2.1 SMA R Nanodiscs

Here, all data was fit using an in-house developed SMALP model based on a core shell bicelle model. Fitted parameter values for nanodiscs with SMA R (A), (B) and (C) and DMPC can be found in Tables S10-S12 and fit graphs in Fig. S14-S16, respectively. In all cases, PDI values were taken from DLS measurements and held.

Table S10 Fit parameters for SMA R (A) nanodiscs.

Parameter	Fit Value
Volume Fraction	0.010 ± 0.005
Mean Core Radius	5.1 ± 0.1 nm
Radial PDI	0.24
Core Length	2.9 ± 0.1 nm
Rim Thickness	0.8 ± 0.1 nm
Mol. Frac. Solvent in Rim	0.10 ± 0.10
SLD Core[a]	$6 \pm 1\times10^{-6}$ Å^{-2}; $-5 \pm 10\times10^{-7}$ Å^{-2}

[a] (left) value for 100% D_2O contrast and (right) for 50% D_2O contrast.

Table S11 Fit parameters for SMA R (B) nanodiscs

Parameter	Fit Value
Volume Fraction	0.010 ± 0.009
Mean Core Radius	5.2 ± 0.1 nm
Radial PDI	0.17
Core Length	3.1 ± 0.2 nm
Rim Thickness	0.8 ± 0.2 nm
Mol. Frac. Solvent in Rim	0.26 ± 0.10
SLD Core[a]	$6 \pm 1\times10^{-6}$ Å^{-2}; $-5 \pm 10\times10^{-7}$ Å^{-2}

[a] (left) value for 100% D_2O contrast and (right) for 50% D_2O contrast.

Table S12 Fit parameters for SMA R (C) nanodiscs

Parameter	Fit Value
Volume Fraction	0.007, 0.024, 0.006
Mean Core Radius	5.5 ± 0.2 nm
Radial PDI	0.18
Core Length	3.3 ± 0.2 nm
Rim Thickness	0.8 ± 0.1 nm
Mol. Frac. Solvent in Rim	0.35 ± 0.20
SLD Core[a]	5.6 ± 1×10^{-6} Å^{-2}; -2.5± 1×10^{-6} Å^{-2}

[a] (left) value for 100% D_2O contrast and (right) for 50% D_2O contrast.

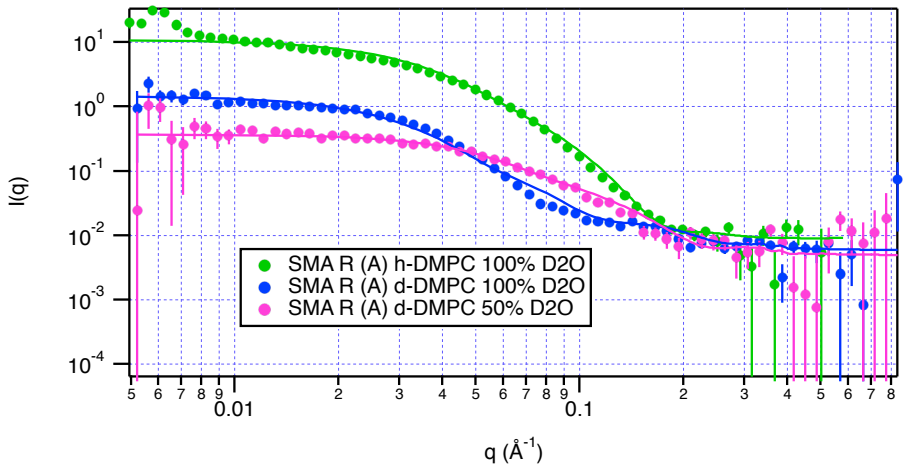

Fig. S14 Fit SANS data for SMA R (A) nanodiscs. (green) SMA R (A) 100% D_2O h-DMPC (blue) SMA R (A) 100% D_2O d-DMPC (pink) SMA R (A) 50% D_2O d-DMPC.

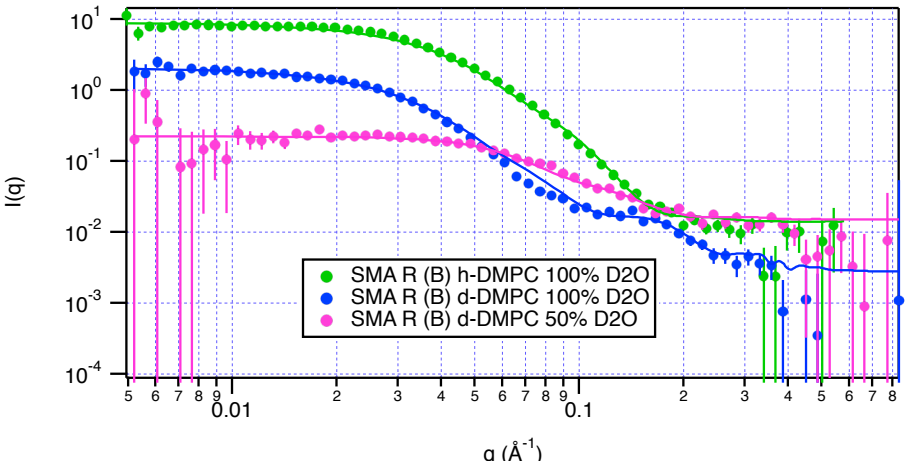

Fig. S15 Fit SANS data for SMA R (B) nanodiscs. (green) SMA R (B) 100% D_2O h-DMPC (blue) SMA R (B) 100% D_2O d-DMPC (pink) SMA R (B) 50% D_2O d-DMPC.

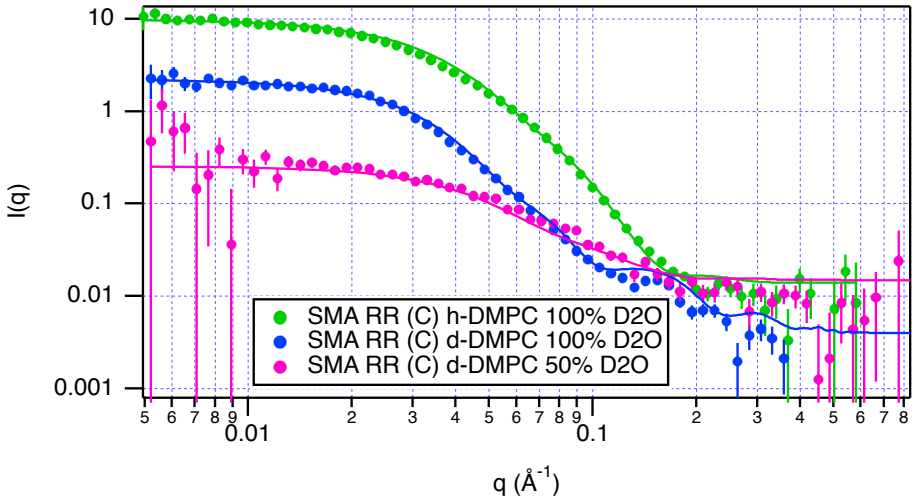

Fig. S16 Fit SANS data for SMA R (C) nanodiscs. (green) SMA R (C) 100% D_2O h-DMPC (blue) SMA R (C) 100% D_2O d-DMPC (pink) SMA R (C) 50% D_2O d-DMPC.

2.9.2.2 SMA RR Nanodiscs

Here, all data was fit using a combined model between the in-house developed nanodisc model, as well as a core shell cylinder with polydisperse radius and length. All fitting was done using the same nanodisc parameters (Table S13), initially fit using SMA RR (A), then held, only fitting aggregate dimensions and concentration (Table S14-S16). PDI values were taken from DLS data and held. Fit graphs can be found in Fig. S17-S19.

Table S13 Fit parameters for SMA RR (A) nanodiscs, which were then held to fit the remainder of the series.

Parameter	Held Value
Mean Core Radius	6.6 ± 0.1 nm
Radial PDI	0.56
Length	2.8 ± 0.1 nm
Rim Thickness	0.9 ± 0.1 nm
h-DMPC core	-5×10^{-7} Å^{-2}
d-DMPC core	6×10^{-6} Å^{-2}
Mol. Frac. Solvent in Rim	0.4 ± 0.2

Table S14 Fit parameters for SMA RR (A) nanodiscs

Parameter	Fit Value
Volume Fraction Nanodiscs	0.010 ± 0.005
Scale Aggregate	0.06 ± 0.02
Aggregate Radius	4.5 ± 0.1
PDI Aggregate Radius	0.21
PDI Aggregate Length	0.21
Aggregate Shell Thickness	0.49 ± 0.01 nm
Aggregate Length	2.96 ± 0.09 nm

Table S15 Fit parameters for SMA RR (B) nanodiscs

Parameter	Fit Value
Volume Fraction Nanodiscs	0.05 ± 0.03
Scale Aggregate	0.09 ± 0.02
Aggregate Radius	4.6 ± 0.1
PDI Aggregate Radius	0.24
PDI Aggregate Length	0.24
Aggregate Shell Thickness	0.49 ± 0.01 nm
Aggregate Length	2.96 ± 0.09 nm

Table S16 Fit parameters for SMA RR (B) nanodiscs

Parameter	Fit Value
Volume Fraction Nanodiscs	0.05 ± 0.02
Scale Aggregate	0.13 ± 0.07
Aggregate Radius	2.5 ± 0.1
PDI Aggregate Radius	0.58
PDI Aggregate Length	0.58
Aggregate Shell Thickness	0.49 ± 0.01 nm
Aggregate Length	2.9 ± 0.1 nm

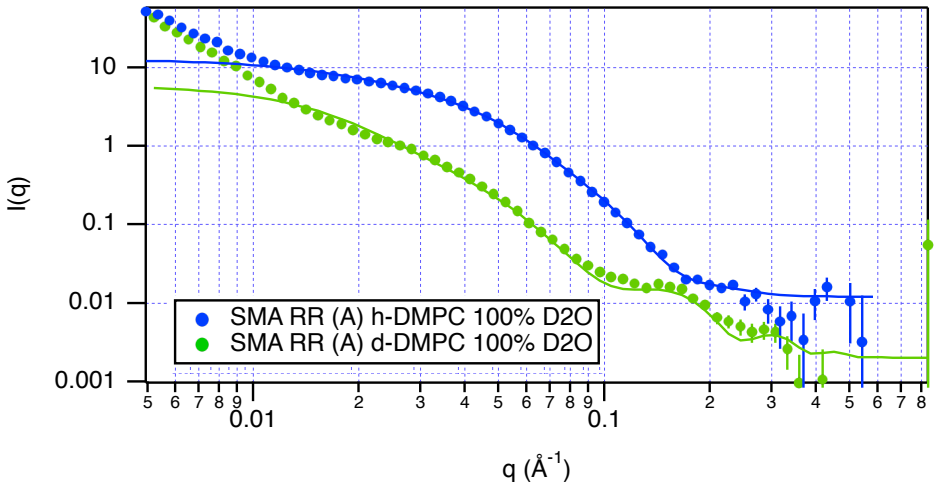

Fig. S17 Fit SANS data for SMA RR (A) nanodiscs. (blue) SMA RR (A) 100% D_2O h-DMPC (green) SMA RR (A) 100% D_2O d-DMPC.

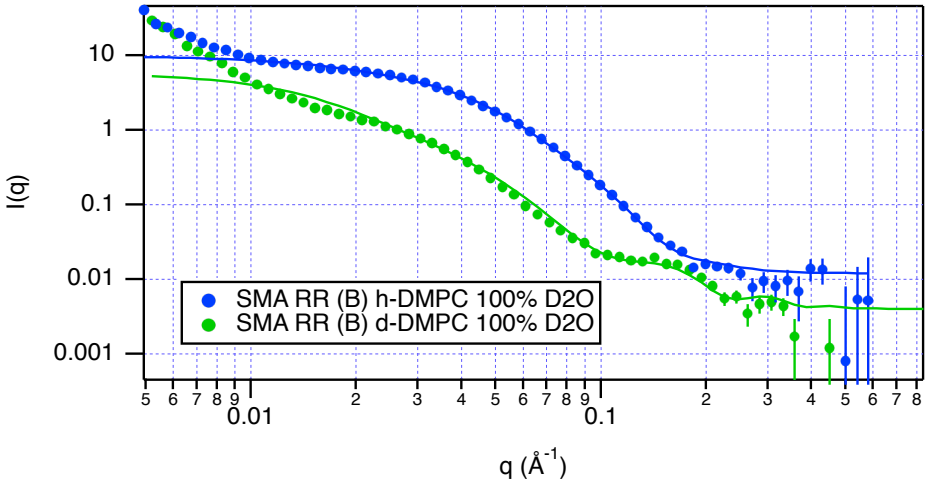

Fig. S18 Fit SANS data for SMA RR (B) nanodiscs. (blue) SMA RR (B) 100% D_2O h-DMPC (green) SMA RR (B) 100% D_2O d-DMPC.

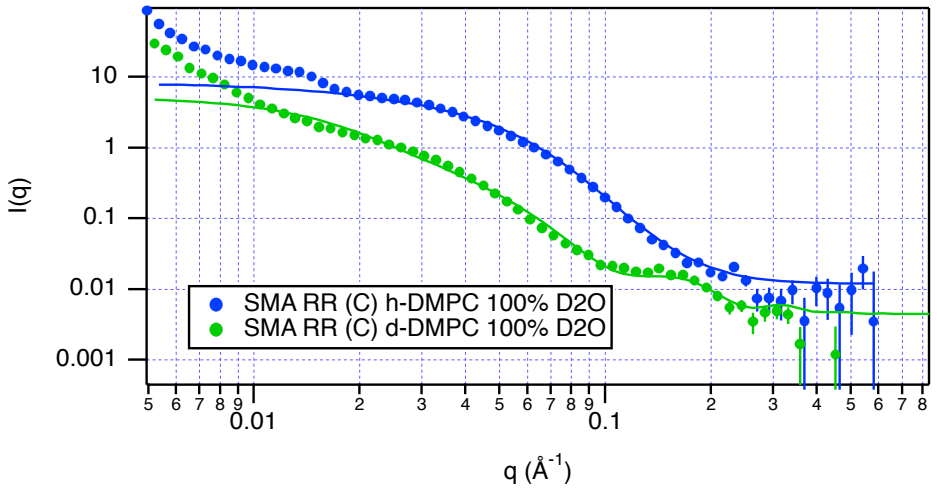

Fig. S19 Fit SANS data for SMA RR (C) nanodiscs. (blue) SMA RR (C) 100% D_2O h-DMPC (green) SMA RR (C) 100% D_2O d-DMPC.

2.5 SAXS

SAXS data was unfortunately not fit within the time-frame of the project. However, data (Fig. S20) could be used in future to verify findings in SANS.

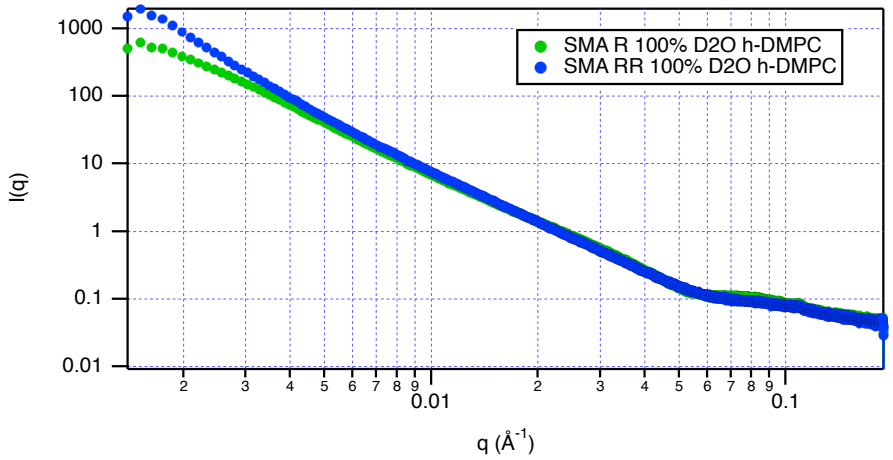

Fig. S20 SASS data for (green) SMA R nanodiscs 100% D_2O h-DMPC and (blue) SMA nanodiscs 100% D_2O h-DMPC.

3.0 References

1. S. Harrisson and K. L. Wooley, *Chem. Commun.*, 2005, 26, 3259–3261.
2. S. C. Hall, C. Tognoloni, G. J. Price, B. Klumperman, K. J. Edler, T. R. Dafforn and T. Arnold, *Biomacromolecules*, 2018, 19, 761-772.
3. M. Chen, G. Moad and E. Rizzardo, *J. Polym. Sci. Part A: Polym. Chem.*, 2009, **47**, 6704–6714.
4. A. F. Craig, E. E. Clark, I. D. Sahu, R. Zhang, N. D. Frantz, M. S. Al-Abdul-Wahid, C. Dabney-Smith, D. Konkolewicz and G. A. Lorigan, Biochimica et Biophysica Acta (BBA)-Biomembranes, 2016, 1858, 2931–2939.
5. O. O. Oyeneye, W. Z. Xu and P. A. Charpentier, *RSC Adv.*, 2015, **5**, 76919-76926.
6. P. F. Barron, D. J. T. Hill, J. H. O'Donnell and P. W. O'Sullivan, *Macromolecules*, 1984, **17**, 1967-1972.
7. M. B. Smith, D. J. McGillivray, J. Genzer, M. Lösche and P. K. Kilpatrick, *Soft Matter*, 2010, **6**, 862–865.